1.E.5: 2.J *Nuclear Physics* **A169** (1971) 275—293; © *North-Holland Publishing Co., Amsterdam*

ON THE ASYMMETRIC DEFORMATION OF FISSIONING NUCLEI

V. V. PASHKEVICH
Joint Institute for Nuclear Research, Laboratory of Theoretical Physics, Dubna

Received 17 February 1971

Abstract: The potential energy of a nucleus at large (scission) deformation is calculated by the shell-correction method due to Strutinsky. The shape of the nucleus in the zeroth-order approximation is taken to be the Cassinian ovaloid, the deviation being expanded in a series of Legendre polynomials. Asymmetric shapes of the nucleus are studied; a definition of the Woods-Saxon type nuclear potential is given; the single-particle spectrum, shell correction, liquid-drop energy and total potential energy are calculated. It is shown that the transuranium nuclei are symmetric at the first barrier and in the second minimum of the potential energy. The second saddle point is situated at a large asymmetric deformation. The nuclear asymmetry near the scission point is in qualitative agreement with experimental data on the asymmetry in the mass distribution of the fission fragments. The agreement between the theoretical results and experimental data on the fission barriers is improved when the asymmetry is taken into account.

1. Introduction

In the theory of fission, the nuclear potential energy is of great importance since its dependence on the shape of the nuclear surface permits both some qualitative conclusions about the fission process to be drawn, and information on the shape and mass of the nucleus in the ground state and the fission barrier to be obtained.

To calculate the potential energy, Strutinsky proposed a method [1-3]) in which the energy is assumed to be a sum of the liquid-drop energy and a shell correction. The value and the sign of the shell correction are determined by the degree of bunching or thinning-out of single-particle levels near the Fermi surface.

To obtain the shell correction for heavy nuclei at large deformations and for hypothetical superheavy nuclei, it is necessary to calculate the single-particle spectrum in a new region of deformations and masses. This spectrum is more or less known only at equilibrium deformation and only near the Fermi surface and has only been fitted to the experimental data on the ground and low-lying excited states of known nuclei.

While extrapolating, it is natural to use nuclear incompressibility and assume the presence of a self-consistent field in the nucleus, approximated by a smooth average field. This field is supposed to have an almost constant value inside the nucleus and in the thin transition layer dropping to zero outside the nucleus. The Woods-Saxon type of potential with the spin-orbit interaction proportional to the potential gradient is the most appropriate one from the physical point of view.

Calculations of the shell correction for an elliptically deformed nucleus, on the basis of the single-particle spectrum in the Woods-Saxon potential, were performed in a paper [4]) by Pashkevich. Strutinsky and his group in Copenhagen [5]) investigated a more general shape of the nucleus with a pronounced neck at large deformations. Earlier, the influence of shells on the fission process was investigated by Ignatyuk [26]) in the model of two tangent fragments.

In the present paper a convenient parametrization of the shape of the fissioning nucleus is proposed. The results of the calculations of the dependence of the potential energy on two parameters, i.e. on the main fission deformation resulting in an increase of the distance between the centers of mass of the would-be fragments and on the asymmetric deformation defining the mass ratio of the future fragments, are given.

The position of the absolute and conditional extrema of the potential energy and their relation to the fission asymmetry are discussed. More detailed calculations are planned to be performed later.

2. Parametrization of the nuclear surface shape

When describing nuclear fission, a convenient parametrization of the shape of a nucleus is a decisive factor determining the amount, and sometimes even the success, of calculations. The determination of parametrization can be divided into two stages. The first one is a choice of the family of basic figures as a zeroth-order approximation, while the second one is a description of the deviation of the figure in question from the basic one.

To specify this deviation, it is sufficient to find a system of coordinates in which the family of basic figures would be coordinate surfaces. Then the deviation would be a function of the coordinates specifying the position of the point on the coordinate surface.

In the case of axial symmetry the deviation is a function of one variable which can be represented as the expansion in a series in orthogonal polynomials. The coefficients of the series are parameters defining the shape of the nuclear surface. Convergence of the series when representing physically interesting functions determines significantly the amount of computation. For example, for the calculation of saddle points in the liquid-drop model, Cohen and Swiatecky [6]) used spheres as figures of the zeroth-order approximation and represented the deviation as a series in Legendre polynomials, 9 terms of the series being taken into account (i.e., even polynomials up to the 18th order). Aside from obvious cumbersomeness, the drawback of this method is that at large deformations, when the nucleus has a pronounced neck, the deviation becomes a multiple-valued function of the polar angle and the series is divergent.

In a paper [7]) by Stavinsky, Rabotnov and Seriogin it was shown that Cassinian ovals are a convenient single-parameter family of curves which surprisingly well ap-

proximate the nuclear shape at the saddle point. In the present paper Cassinian ovals are used as figures of the zeroth-order approximation and the deviation from these is represented as a series in Legendre polynomials.

Let us restrict ourselves to axially symmetric figures and in the plane going through the axis of symmetry introduce coordinates (R, x) such that the coordinate line $R = \text{const}$ is a Cassinian oval, $0 \leqq R < \infty$, and x is confined as follows: $-1 \leqq x \leqq 1$. The (R, x) coordinates are related to the cylindrical coordinates $(\bar{r}, \bar{z})$ by the expressions

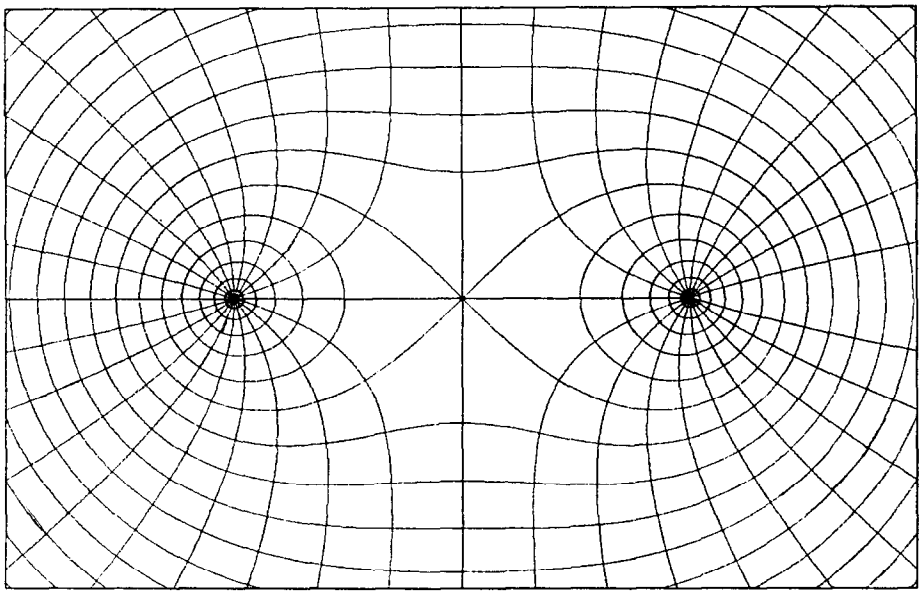

Fig. 1. Curvilinear system of orthogonal (R, x) coordinates. The lines $R = \text{const}$ are Cassinian ovals, the lines $x = \text{const}$ start from the left (at $x < 0$) or right (at $x > 0$) foci and go to ∞.

$$R = [(\bar{z}^2+\bar{r}^2)^2-2s(\bar{z}^2-\bar{r}^2)+s^2]^{\frac{1}{4}},$$

$$x = \frac{\operatorname{sign}(\bar{z})}{\sqrt{2}}\left\{1+\frac{\bar{z}^2-\bar{r}^2-s}{[(\bar{z}^2+\bar{r}^2)^2-2s(\bar{z}^2-\bar{r}^2)+s^2]^{\frac{1}{2}}}\right\}^{\frac{1}{2}}, \tag{1}$$

where s is the squared distance from the focus of Cassinian ovals to the origin of coordinates, a quantity fixed for any coordinate grid. For $s = 0$ the (R, x) coordinates change to polar coordinates, or more precisely, to the radius and cosine of the polar angle. For $s \neq 0$, the coordinate grids differ one from another only in scale.

One such coordinate grid is presented in fig. 1. The coordinate line $R = \text{const}$ (Cassinian oval) at $0 < R < \sqrt{s}$ consists of two separate closed curves tending at $R \to 0$ to circumferences centered at the left and right foci, and at $\sqrt{s} < R < \infty$ it is a single curve tending at $R \to \infty$ to a circle centered at the origin. The coordinate line $R = \sqrt{s}$ is a Bernoulli lemniscate.

The coordinate line $x = \text{const}$ at $x > 0$ ($x < 0$) leaves the right (left) focus and tends to infinity approaching a straight line drawn through the origin.

The transformation, inverse to (1), has the form

$$\bar{r} = \frac{1}{\sqrt{2}}\left[(R^4+2sR^2(2x^2-1)+s^2)^{\frac{1}{2}}-R^2(2x^2-1)-s\right]^{\frac{1}{2}},$$

$$\bar{z} = \frac{\operatorname{sign}(x)}{\sqrt{2}}\left[(R^4+2sR^2(2x^2-1)+s^2)^{\frac{1}{2}}+R^2(2x^2-1)+s\right]^{\frac{1}{2}}. \tag{2}$$

Let us consider such a curve in the (R, x) plane that the coordinate lines $x = \text{const}$ intersect it at no more than one point. We denote the value of R at which the intersection takes place by $R(x)$ and represent the function $R(x)$ in the equation for the curve $R = R(x)$ as a series in Legendre polynomials:

$$R(x) = R_0(1+\sum_m \alpha_m P_m(x)). \tag{3}$$

We shall study the properties of an axially symmetric nucleus, the surface of which is presumed to be generated by the rotation of the curve (3). As a measure of the deformation of the figures of the zeroth-order approximation, it is convenient to introduce a dimensionless quantity ε, such that

$$s = \varepsilon R_0^2.$$

3. Geometrical characteristics

While calculating such geometrical quantities as the volume of the nucleus, the center of mass, quadrupole moment etc., we assume that the nuclear density is constant in the internal region bounded by the surface (3) and is zero outside it. The Coulomb potential is calculated under the assumption that the charge density is proportional to the nuclear density.

Convenient integral expressions for those quantities in cylindrical coordinates are given in a paper [8]) by Strutinsky, Lyashchenko and Popov. Using (1) and (2) it is possible to find an implicit equation for the curve in cylindrical coordinates. But there arise two complications. First, it is necessary to solve numerically the implicit equation. Second, and what is more important, the solution $\bar{r} = \bar{r}(\bar{z})$ of the equation becomes multiple-valued for the α_{2m} parameters, $m = 1, 2, \ldots$, equal or less than some critical negative values. Near these critical values the curve meets the axis $\bar{r} = 0$ with a large derivative $\mathrm{d}\bar{r}^2/\mathrm{d}\bar{z}$, so that the accuracy of the calculation of the integrals sharply decreases when the integration is carried out by the Gauss method with a fixed number of knots. It is more in line with the present development to evaluate the integrals in the (R, x) coordinates, taking x as an independent variable. Expressions for the integrals in the (R, x) coordinates are given in the appendix.

It is obvious that the volume of the defined figure changes with the (ε, α_m) parameters. The center of mass is also displaced as the α_{2m-1}, $m = 1, 2, \ldots$, vary. Let us perform a linear stretching of the figure and shift it along the z-axis in such a way that the volume of a new figure would remain constant and the center of mass would be fixed at the origin of the coordinates with any change of the values of the (ε, α_m) parameters.

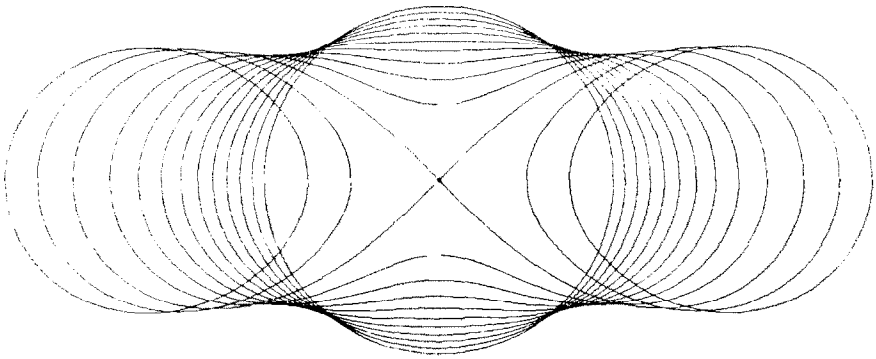

Fig. 2. Cassinian ovals are a single-parameter family of curves convenient to approximate the nuclear surface shape. The volume is conserved. The parameter ε varies from 0 (sphere) through 1.2 with a step of 0.1 ($\varepsilon = 1.1$ and 1.2 correspond to the separated fragments). At $\varepsilon = 1.0$ (Bernoulli lemniscate) the curve has a double point at the centre of symmetry.

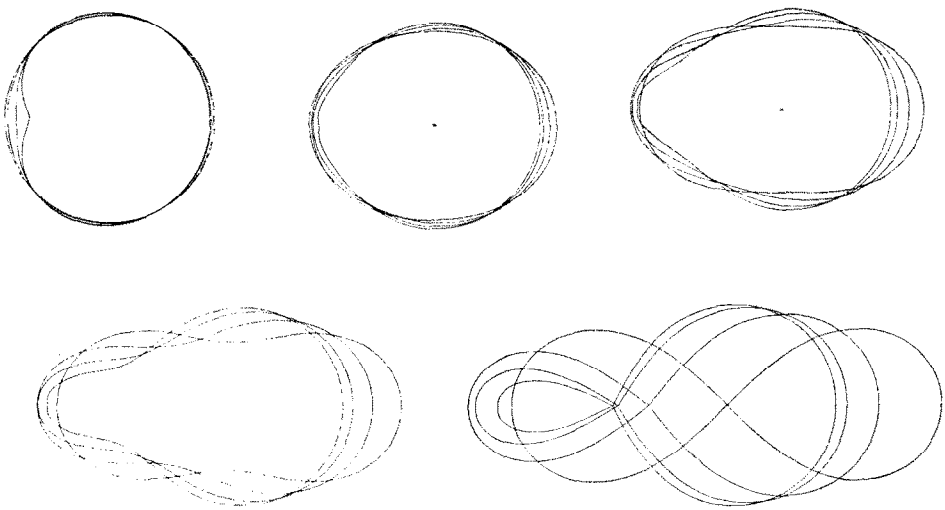

Fig. 3. Cassinian ovals perturbed by "dipole" ($\alpha_1 \neq 0$) deformation. $\varepsilon = 0.0$, 0.25 and 0.50 correspond to the figures in the upper row, $\varepsilon = 0.75$ and 1.00 to the lower row. In each figure, the curves corresponding to $\alpha_1 = 0.0$, 0.1, 0.2, 0.3 intersect the horizontal axis of symmetry to the right from the origin at the points maximally separated from the origin at $\alpha_1 = 0$ and approaching it with increasing α_1. The origin is marked by a cross.

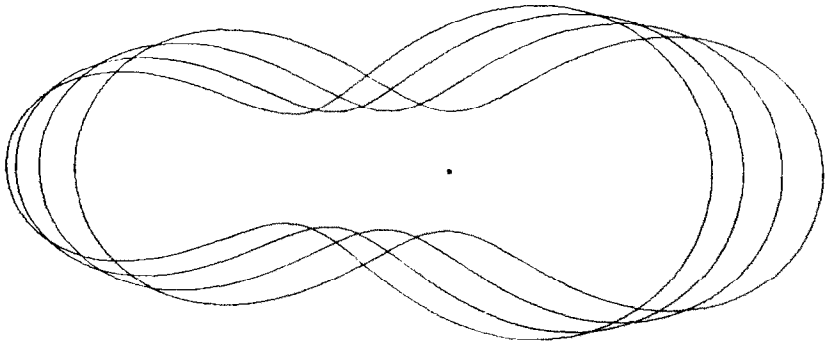

Fig. 4. The same as in fig. 3 at $\varepsilon = 0.95$.

To illustrate this, fig. 2 shows the shape of the nucleus in the zeroth-order approximation, i.e. for $\alpha_m = 0$, $m = 1, 2, \ldots$. The scale of the figures is arbitrary. A spherical shape of the nucleus corresponds to the value $\varepsilon = 0$. For $0 < \varepsilon < 0.4$ Cassinian ovals are very close to ellipses with the ratio of half-axes

$$\frac{(1-\frac{2}{3}\varepsilon)}{(1+\frac{1}{3}\varepsilon)}.$$

As ε increases from 0.5 to 1.0, there appears and becomes progressively thinner a neck, which at $\varepsilon = 1.0$ goes to zero. With a further increase of ε, the fragments are separating from each other, their shape approaching a spherical one.

A more complicated nuclear shape asymmetric under reflection at the plane perpendicular to the axis of symmetry is represented in fig. 3, where each separate picture shows the figures for fixed ε, $\varepsilon = 0.0(0.25)1.00$ †, and four values of α_1, $\alpha_1 = 0.0(0.1)0.3$. At $\varepsilon = 0$, the α_1 parameter describes dipole deformation of the sphere which, as is well known, at small α_1 mainly leads to the displacement of the center of mass. Therefore when α_1 varies and the center of mass is kept fixed the nuclear shape does not change significantly. At $\varepsilon \neq 0$, a change of the α_1 parameter cannot already be reduced to a dipole deformation and with the growth of ε the nuclear shape becomes increasingly dependent on α_1.

As α_1 varies, the ratio of the volumes of the "future fragments" changes. It is a convenient feature of the present parametrization that at $\varepsilon \approx 0.8$–1.0, as is seen from the figures, the heavy "fragment" is close to a spherical shape, whereas the light "fragment" remains deformed.

4. Nuclear potential

A definition of the radial dependence of the potential of a deformed nucleus with an arbitrary shape of the surface, convenient from the point of view of calculations,

† Here and in the following we shall use the notation $x = x_i(\Delta x)x_f$ which means that x goes from x_i through x_f with step Δx.

was proposed by Pashkevich [4]). It differs from the integral expression for the potential of Bolsterli *et al.* [9]) in simplicity but gives close results.

Let us define at a point with the cylindrical (r, z) coordinates a function $\Phi(r, z)$,

$$\Phi(r, z) = [(\bar{z}^2+\bar{r}^2)^2-2\varepsilon R_0^2(\bar{z}^2-\bar{r}^2)+\varepsilon^2 R_0^4]^{\frac{1}{2}}-R_0[1+\sum_m \alpha_m P_m(x)],$$

where

$$\bar{r} = rc,\ \bar{z} = zc+\bar{z}_m,\ R_0 = r_0 A^{\frac{1}{3}},$$

and the x-coordinate of the point is related to the cylindrical $(\bar{r}, \bar{z})$ coordinates by the transformation (1). The stretching coefficient c and displacement $\bar{z}_m$ responsible for the constant volume and fixed center of mass are defined in the appendix.

The equation

$$\Phi(r, z) = 0 \tag{4}$$

defines the nuclear surface in cylindrical coordinates. Then the nuclear potential can be given as follows [4])

$$V = V_0[1+\exp(\Psi/a)]^{-1}. \tag{5}$$

The quantity Ψ, which can be interpreted as an approximation to the distance between a point and the nuclear surface, has the form

$$\Psi(r, z) = \frac{\Phi}{|\nabla\Phi|} = \frac{\Phi[(\bar{z}^2+\bar{r}^2)^2-2s(\bar{z}^2-\bar{r}^2)+s^2]^{-}}{c(\bar{r}^2N_r^2+\bar{z}^2N_z^2)^{\frac{1}{2}}}, \tag{6}$$

where the following notations are used:

$$N_r = (\bar{z}^2+\bar{r}^2+s)[(\bar{z}^2+\bar{r}^2)^2-2s(\bar{z}^2-\bar{r}^2)+s^2]^{\frac{1}{2}}+\bar{z}^2(\bar{z}^2+\bar{r}^2-s)[R_0\sum_m \alpha_m P'_m(x)/N_x],$$

$$N_z = (\bar{z}^2+\bar{r}^2-s)[(\bar{z}^2+\bar{r}^2)^2-2s(\bar{z}^2-\bar{r}^2)+s^2]^{\frac{1}{2}}-\bar{r}^2(\bar{z}^2+\bar{r}^2+s)[R_0\sum_m \alpha_m P'_m(x)/N_x],$$

$$N_x = \frac{\text{sign}(\bar{z})}{\sqrt{2}}\{[(\bar{z}^2+\bar{r}^2)^2-2s(\bar{z}^2-\bar{r}^2)+s^2]^{\frac{1}{2}}+(\bar{z}^2-\bar{r}^2-s)\}^{\frac{1}{2}}.$$

Here $P'_m(x)$ is the derivative of the Legendre polynomial with respect to x.

The implicit expression (4) for the nuclear boundary is chosen in such a way that at $\varepsilon = 0$, and, consequently, $s = 0$, the potential (5) turns into the Woods-Saxon potential of the spherical nucleus.

The spin-orbit interaction was chosen to be proportional to the gradient of the potential (5) with the $r_{s.o.}$ parameter used instead of r_0, and $r_{s.o.} < r_0$ (see the paper [10]) by Rost).

$$V_{s.o.} = \frac{2k}{\hbar^2}[\boldsymbol{s}, \boldsymbol{p}]\nabla V, \qquad k = \lambda\left(\frac{\hbar}{2Mc}\right)^2, \tag{7}$$

where $\boldsymbol{p}$ and $\boldsymbol{s}$ are the nucleon momentum and spin.

The calculation of the Coulomb potential is described in the appendix.

We assume that such parameters of the average field as the depth of the potential well V_0, its diffuseness a, the strength of the spin-orbit interaction k and the parameters r_0 and $r_{s.o.}$ do not vary much with deformation and that these variations can be neglected when studying the dependence of the total nuclear energy on the shape of the nuclear surface. In our numerical calculation we used for these parameters the values of Rost [10]) fitted to the experimental data on the single-particle levels of nuclei close to ^{208}Pb (see table 1). The isospin dependence of the depth of the potential well V_0 was taken [11-13]) to be

$$V_0^{(p,n)} = V_{mean}\left(1 \pm C_{iso}\frac{(N-Z)}{A}\right).$$

The method of calculating a single-particle spectrum is described in papers [14,15]).

TABLE 1

The parameters of the potential [10])

	Protons	Neutrons
r_0 (fm)	1.275	1.347
$r_{s.o.}$ (fm)	0.932	1.28
a (fm)	0.700	0.700
λ	17.8	31.5
V_{mean} (MeV)	49.65	
C_{iso}	0.862	

5. Shell correction

On the basis of the single-particle spectrum obtained, proton and neutron shell corrections were calculated using the computer routine written by Strutinsky and Pauli. As an illustration, fig. 5 shows shell corrections for neutrons and protons versus number of nucleons and asymmetric deformation α_1 in the form of topographic maps. The value of the parameter ε is fixed and equal to 0.95.

The regions of negative values of the shell correction corresponding to the increased stability of the nucleus are shaded. To appreciate the influence of the parameter α_1 on the nuclear shape, in fig. 5 a grid of curves is traced with thin lines along which the volume (i.e. the number of nucleons) of a future fragment remains the same. The boundary between the two fragments was determined by that plane perpendicular to the symmetry axis which has the minimal area cross section with the figure.

The nuclear shape for which the shell corrections discussed above were calculated is given in fig. 4. As is seen, the deformation $\varepsilon = 0.95$ corresponds to well-pronounced fragments connected with a thin neck so that in the shell correction one may well expect the influence of the single-particle spectrum of each fragment separately.

Of course, this influence is distorted both by the interaction of the fragments through the neck and their deformation. Nevertheless, as one can see from fig. 5 there exists a deep valley in the shell correction for protons between the lines corresponding to 50 and 60 protons in the heavy fragment. The fact that the valley follows the lines of constant number of nucleons in the heavy fragment suggests that it is the heavy fragment which is responsible for its appearance.

The valley between 20 and 30 protons in the light fragment is less pronounced but quite noticeable. There is a deep minimum at an intersection of these valleys, i.e. in the proton system with $Z = 78$ and at the deformation $\alpha_1 = 0.175$ which corresponds

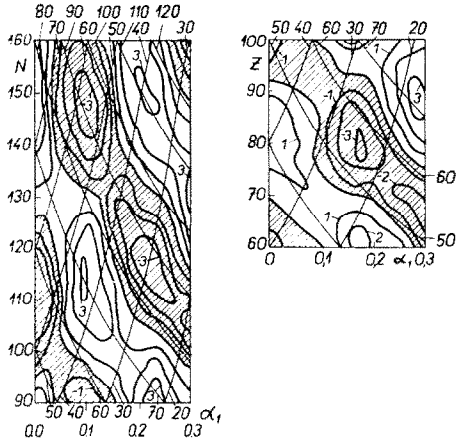

Fig. 5. The shell correction for neutrons (left) and protons (right). The dependence on "dipole" deformation α_1 and the number of nucleons is represented in the form of a topographical map. The lines of the constant shell correction (thick curves) are drawn with an interval of 1 MeV. The regions where the shell correction is negative are shaded. The curves along which the number of nucleons is constant in the light (the lines going upwards to the right) and heavy (the lines going upwards to the left) fragments are marked by thin lines. The numbers which are multiples of 10 in the upper and (only for neutrons) lower horizontal rows denote the number of nucleons in the fragments. The numbers in the right vertical column denote the total number of nucleons.

to the division into two "magic" fragments with 24 and 54 protons. I would like to emphasize that the mathematical division into two fragments introduced here is not the physical scission. The latter is influenced not only by the shell correction, but also by many other factors, among them are the liquid-drop energy and the difference between the deformation at which the scission actually takes place and that considered here.

The valley for the heavy fragment is more pronounced than that for the light one. Apparently, this is due to the fact that, as is seen from fig. 4, the shape of the light fragment differs more significantly from the sphere and its single-particle field is more distorted by the presence of the neck, than it is for the heavy one. Besides, it is well known that the larger is the number of nucleons the deeper are the known magic dips in the energy of spherical nuclei.

Similarly, in the shell correction for neutrons one can see the "interference" of the valleys of the heavy (between 50 and 60, 80 and 90 and above 120 neutrons) and light (in the region of 30 and between 50 and 60 neutrons) fragments.

Thus, the shell correction is important not only for the equilibrium deformation and the second minimum in the nuclear potential energy but also at the larger deformations up to the point of scission of the nucleus where it changes smoothly into a sum of the shell corrections for the two fragments. In addition, the proximity of the above-mentioned "magic" numbers in the fragments to the known spherical magic numbers 28, 50, 82, 126 indicates that the chosen two-parameter family of figures rather successfully approximates the nuclear shape. In the framework of this parametrization one can study the continuous transition from the nuclear ground state to the scission point.

6. Nuclear potential energy. Main results

As is well known, in the Strutinsky method [1-3]) the nuclear potential energy is considered to be a sum of the liquid-drop energy and the shell correction

$$W = W^{\text{l.d.}} + \sum_{\text{p, n}} \delta U^{(\text{p, n})}. \tag{8}$$

The shell correction was discussed in the previous section. The part of the liquid-drop energy dependent on deformation can be written as

$$W^{\text{l.d.}} = \sigma A^{\frac{2}{3}} \left[f_{\text{s}} + 2 \frac{Z^2/A}{(Z^2/A)_{\text{cr}}} f_{\text{C}} \right], \tag{9}$$

where

$$f_{\text{s}} = B_{\text{s}} - 1.0, \qquad f_{\text{c}} = B_{\text{c}} - 1.0.$$

The parameters σ and $(Z^2/A)_{\text{cr}}$ were taken to be 16 MeV and 45, respectively, according to the choice of Strutinsky [1, 3]). Expressions for the surface area B_{s} and Coulomb energy B_{C} are given in the appendix.

As an example, fig. 6 presents the results of the calculations of $W^{\text{l.d.}}$ for ^{236}U as a function of α and α_1. The parameters α and ε are related by the expression

$$\varepsilon = \frac{\alpha - 1}{4} \left[\left(1 + \sum_m \alpha_m\right)^2 + \left(1 + \sum_m (-1)^m \alpha_m\right)^2 \right] + \frac{\alpha + 1}{2} \left[1 + \sum_{m=1} (-1)^m \alpha_{2m} (2m-1)!!/(2^m m!) \right]^2, \tag{10}$$

which is chosen in such a way that the neck thickness becomes equal to zero at $\alpha = 1$ for any value of the parameters α_m, $m = 1, 2, \ldots$. At $\alpha_m = 0$, $m = 1, 2, \ldots$, $\alpha = \varepsilon$.

From fig. 6 one can see that, as is well known, in the liquid-drop model the shape of the fissioning nucleus is symmetrical under reflection at the plane perpendicular to the axis of symmetry of the nucleus and going through the nuclear center of mass.

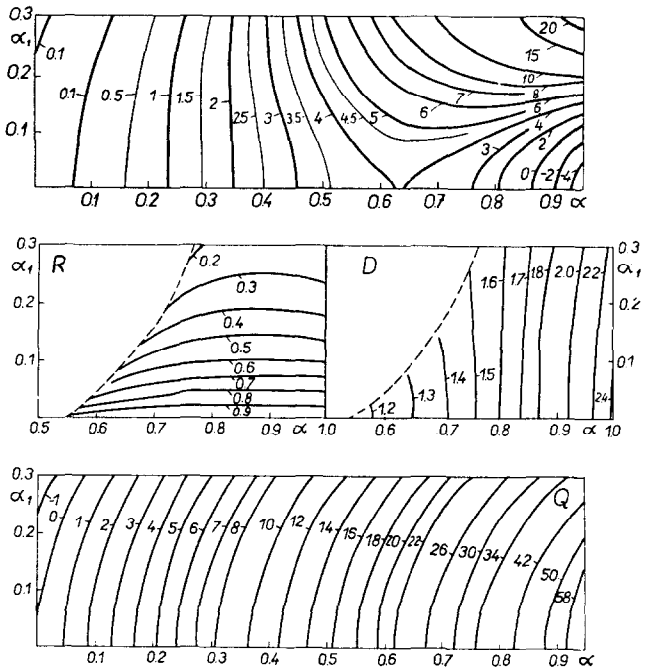

Fig. 6. The dependence on the parameters α and α_1, given in the form of topographical maps, of the following quantities. Top: the energy of the ^{236}U nucleus (in MeV) in the liquid-drop model defined by (9). Centre left: the ratio of the volumes of the light to the heavy fragments. Centre right: the distance between the centres of mass of the fragments. (In units of the radius of the sphere of equal volume R_0.) Bottom: the quantity proportional to the nuclear quadrupole moment Q (the definition is given in the appendix). The numbers attached to the constant level lines are the values of Q multiplied by 10.

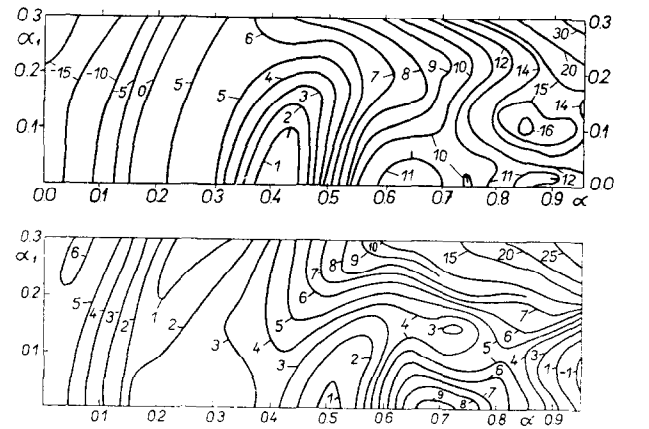

Fig. 7. The dependence on the parameters α and α_1, given in the form of topographical maps, of the total energy (in MeV) for ^{208}Pb at the top and ^{230}Th at the bottom.

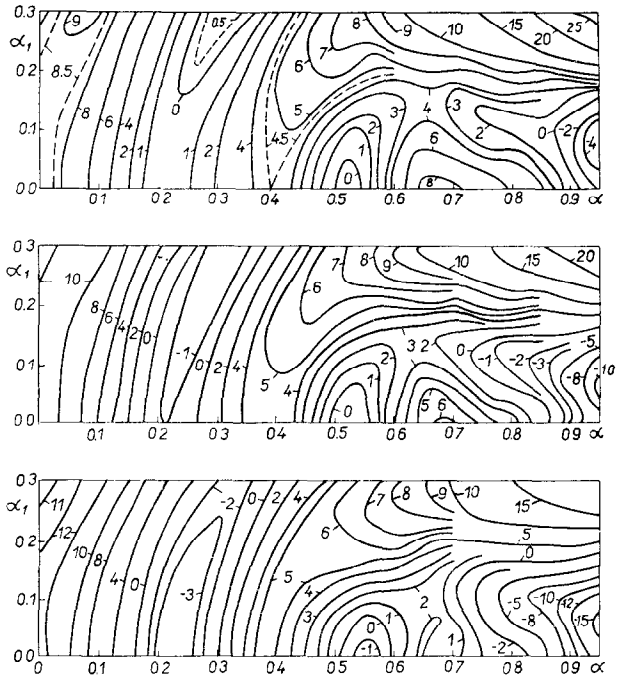

Fig. 8. The same as in fig. 7 for ^{236}U at the top, ^{240}Pu in the middle and ^{252}Cf at the bottom.

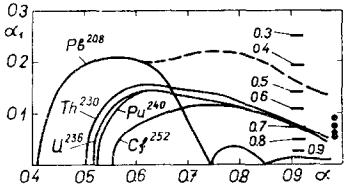

Fig. 9. The position of the bottom of the valleys leading from the second minimum to the scission through the second saddle point. For ^{208}Pb there are two valleys, the higher one is marked by the dashed line. The scale of the ratio of the masses of the light to the heavy fragment is given at $\alpha = 0.9$. The points represent the experimental ratios of the masses of the light to heavy fragments for the most probable fission of the nuclei ^{232}Th, ^{235}U, ^{239}Pu and ^{252}Cf, from top to bottom, respectively [19–22]).

The results of the calculations of the total energy for a number of nuclei are presented in figs. 7 and 8. To discuss them in physical terms, one should relate the parameters used with the known nuclear characteristics.

At sufficiently large values of α ($\alpha \approx 0.6$–0.7) there appears a neck in the nucleus, i.e. the cylindrical coordinate r of a point at the surface as a function of z reaches its minimum at a certain $z = z^*$. Then it becomes possible to introduce new characteristics of the shape associated with the geometrical division of the nucleus by the plane $z = z^*$ into two fragments. Having calculated the volume and the center

of mass of the both fragments, we can introduce the distance between the centers of mass of the fragments D and the ratio of the fragment volumes R_m. The dependence of D and R_m on the parameters α and α_1 is shown in fig. 6. As is seen, it is the distance between the centers of mass of the fragments D that is mainly changing with the growth of α, the ratio of the fragment masses R_m being comparatively constant. Similarly, α_1 mainly determines R_m. Had the quantities D and R_m a sense in the entire region of variations of the parameters α and α_1, they could have been taken as convenient from the physical point-of-view parameters instead of α and α_1.

With the growth of deformation, as is seen from figs. 2, 3 and 4, the nucleus becomes more and more stretched, resulting in an increase of the nuclear quadrupole moment Q. The dependence of Q on (α, α_1) calculated by formula (A.15) is given in fig. 6. With increasing α_1 at fixed α the nuclear asymmetry grows, the nuclear shape becomes closer to a sphere and the quadrupole moment is decreased, which results in a deviation of the lines of constant Q to the right. The replacement of the variable ε by α has the same effect.

Let us now return to the main results of this paper presented in figs. 7 and 8. At small deformations, the nuclear shape is weakly dependent on α_1 (see fig. 3). The lines of constant total potential energy essentially follow those of the quadrupole moment Q, i.e. at small α the total energy is mainly determined by the nuclear quadrupole moment.

Small deviations from this dependence, stability or instability of the ground state against asymmetric deformation may not be discussed here, since it is well known that in heavy nuclei, especially in Th and U, nuclear hexadecapole deformation [16]) is of great importance. Inclusion of this deformation affects significantly (up to 2 MeV) the depth of the ground state minimum of the potential energy.

At deformations $\alpha \approx 0.4$–0.5, the nuclear shape becomes significantly dependent on α_1 (see figs. 3 and 4) and the lines of constant W lose all the resemblance to those of constant Q.

From the figures one can see that the saddle point for the transition from the ground state to the second minimum is situated for all the nuclei at symmetric deformation ($\alpha_1 = 0$). The second minimum of the potential energy is stable against α_1 so that up to the deformation α corresponding to the second minimum, inclusion of asymmetric deformation gives nothing new. The height of the second minimum above the ground state is not discussed here, since the depth of the ground state is not calculated properly (see above).

After the second minimum in W the valley leading to the second saddle point sharply deviates from the axis $\alpha_1 = 0$ and the saddle point is situated at considerable asymmetric deformation.

Inclusion of asymmetric deformation lowers considerably the second saddle point, so that in the transuranium nuclei it falls down below the first one, in agreement with the experimental data. The relative height of the two saddle points is discussed by Bjørnholm and Strutinsky [17]) where there are further references to the

experimental papers. As a result of the calculation with $\alpha_1 \neq 0$ the theoretical fission barriers are in better agreement with the experimental ones.

After the second saddle point, the position of the conditional minimum at fixed α moves with the increase of α towards a decrease of asymmetry. We want to connect the calculated values of asymmetric deformation with the asymmetry of the mass distribution of the fission fragments. Here a number of difficulties arise and the final answer can be obtained only after solving a dynamical problem. Without knowing a measure of the adiabaticity and inertness of the collective motion during the transition from the saddle point to scission, one can only hope that the descent in low-energy fission takes place near the bottom of the valley W.

As was shown by Strutinsky, Lyashchenko and Popov [8]) in the liquid-drop model, the nucleus at a certain critical deformation and still with a sufficiently thick neck becomes absolutely unstable against the scission into two fragments. Fig. 4 presents the nuclear shapes which are close to the critical one in the ratio of the thickness of the neck to the distance between the centers of mass of the fragments. The division of the nucleus with a sufficiently thick neck and the influence of the uncertainty in the location of the point of scission on the charge and mass distributions of fragments was discussed in close connection with the experimental data on the fission of excited nuclei by Karamian, Oganesian and Pustyl'nik [18]). Since, according to figs. 7 and 8, the asymmetry depends on α, the uncertainty of deformation at which the scission takes place introduces uncertainty in the ratio of the fragment masses.

Keeping in mind the foregoing reservations, let us compare the experimental data [19-22]) on the ratio of masses of the most probable fragments with the theoretical values. Fig. 9 shows the position of the bottom of the valley leading from the second minimum to the saddle point and further to the scission. As was mentioned above, the asymmetry at the saddle point is rather large and exceeds the experimental one.

From the saddle point to scission, the asymmetry (along the bottom of the valley) decreases and at the scission point becomes a little smaller than the experimental value. Thus, in the process of fission R_m changes from approximately 0.5 to 0.8 and, in view of the uncertainties mentioned, that may be considered to be in satisfactory agreement with the values observed. Unlike the experimental situation, similar values of R_m are obtained for all the nuclei. The reason can be understood from a comparison of the α_1 dependence of the shell corrections and the liquid-drop energy. In the region of the saddle point, the rate of the variation of the shell correction (comparable with the example given in fig. 5 for $\alpha = 0.95$) is of the same order as that of the liquid-drop energy (see fig. 6). And in the total energy a decrease of asymmetry with the number of nucleons manifests itself as it is observed experimentally. In the vicinity of the scission point the liquid-drop energy steeply increases with α_1, suppressing nuclear individuality which originates from the shell correction.

In the region of Pb, where the shell correction for both protons and neutrons reaches a deep minimum at considerable asymmetric deformation, there exist two saddle points which are situated near the scission point: one corresponds to very

small and the other to quite considerable asymmetry. The "symmetric" saddle point lies below the "asymmetric" one that favours the symmetric fission in agreement with the experimental data on the fission of nuclei close to ^{208}Pb [ref. [23])]. It is of interest to note that the experimentally observed small peak in the mass distribution in the fission of ^{209}Bi induced by 36 MeV protons [24]) at $R_m = 0.5$ is close in asymmetry to the upper saddle point ($R_m = 0.48$).

The main results obtained in this section are in qualitative agreement with the results of Strutinsky's group in the Niels Bohr Institute in Copenhagen [5]), though there is a difference in the parametrization of the shape of the nuclear surface and the parameters of the average field used. That suggests that in the fission process it is not the details of the surface shape but such characteristics as the distance between the centers of mass, the neck thickness and the ratio of the volumes of the future fragments that are of primary importance.

The fact that the second saddle point is located at an asymmetric deformation of the nucleus was also obtained by Möller and Nilsson [25]) (see also ref. [27])). For an average field these authors used the infinite oscillator potential with usual corrections proportional to $\boldsymbol{l}^2 - \bar{\boldsymbol{l}}^2$ the meaning of which at such large deformations is not obvious.

7. High-order deformations

So far the results of the study of the dependence of W on two parameters α and α_1 have been presented. As has been mentioned in the previous section, α_4 is the most important of the remaining parameters. It affects both the nuclear shape in the ground state and the deformation of the fragments before their separation. Preliminary calculations show that inclusion of α_4 results in the stability of the ground state against α_1, changes W a little in the region of the second minimum and lowers the second barrier for symmetric fission ($\alpha_1 = 0$), so that the gain in energy from the inclusion of α_1 somewhat decreases.

The role of the parameter α_2 is not large, since it is strongly correlated with α.

8. Conclusion

The nucleus is symmetric at the first barrier and the second minimum of the total potential energy. Asymmetry becomes essential near the second saddle point, which thereby corresponds to the asymmetric shape of the nucleus. Addition of the shell corrections to the liquid-drop energy leads to the fact that the conditional minimum of the potential energy at a fixed distance between the centers of mass of the future fragments lies at non-zero asymmetric deformation of the nucleus.

With the growth of the distance between the centers of mass of the future fragments, the ratio of masses of the fragments sharply increases on the path from the second minimum to the second saddle point and then smoothly decreases, approximately reaching near the point of scission the experimental values.

The remaining difference between the theoretical and experimental values may be ascribed both to uncertainties of principal character and to the lack of variations of high-order deformation of the future fragments.

Thus, it was shown that the nucleus in the process of fission has non-zero asymmetric deformation which is certainly important both for (i) a qualitative understanding of asymmetry in the mass distribution of fragments and (ii) from the point-of-view of principle.

The author wishes to thank cordially V. M. Strutinsky for numerous useful discussions. The author is also grateful to the members of Strutinsky's group in the Niels Bohr Institute in Copenhagen for furnishing the results of their calculations prior to publication.

The author is grateful to V. G. Soloviev for his continuous interest in the work, and to D. A. Arseniev, P. E. Vorotnikov, A. V. Ignatyuk, Yu. A. Muzychka and B. I. Pustyl'nik for stimulating discussions. Regular consultations with I. N. Silin contributed much to the general level of the routines used in the calculations. Shell corrections were calculated using the routines written by Strutinsky and Pauli. It is pleasure for the author to mention invaluable assistance of the operators under L. S. Pervushova when performing calculations on the BESM-6 computer.

Appendix

For efficient use of the computer time, it is convenient to calculate a number of integrals in a group method together with the calculation of the volume of the figure.

Using eqs. (3) and (2), we express the integrands dependent explicitly on r and z as functions of x. Thus

$$\mathrm{d}\bar{z} = \left(\frac{\partial \bar{z}}{\partial x} + \frac{\partial \bar{z}}{\partial R}\,\frac{\mathrm{d}R}{\mathrm{d}x}\right)\mathrm{d}x,$$

$$\mathrm{d}\bar{z}\,\frac{\mathrm{d}\bar{r}}{\mathrm{d}\bar{z}} = \left(\frac{\partial \bar{r}}{\partial x} + \frac{\partial \bar{r}}{\partial R}\,\frac{\mathrm{d}R}{\mathrm{d}x}\right)\mathrm{d}x,$$

where $\mathrm{d}R/\mathrm{d}x$ is obtained by differentiating equation (3) and

$$\frac{\partial \bar{z}}{\partial x} = \sqrt{2}|x|R^2(s+p)p^{-1}[p+R^2(2x^2-1)+s]^{-\frac{1}{2}}, \tag{A.1}$$

$$\frac{\partial \bar{r}}{\partial x} = \sqrt{2}xR^2(s-p)p^{-1}[p-R^2(2x^2-1)-s]^{-\frac{1}{2}}, \tag{A.2}$$

$$\frac{\partial \bar{z}}{\partial R} = \frac{\operatorname{sign}(x)}{\sqrt{2}}\,R[R^2+(2x^2-1)(s+p)]p^{-1}[p+R^2(2x^2-1)+s]^{-\frac{1}{2}}, \tag{A.3}$$

$$\frac{\partial \bar{r}}{\partial R} = \frac{1}{\sqrt{2}} R[R^2+(2x^2-1)(s-p)]p^{-1}[p-R^2(2x^2-1)-s]^{-\frac{1}{2}}, \tag{A.4}$$

$$p = [R^4+2sR^2(2x^2-1)+s^2]^{\frac{1}{2}}. \tag{A.5}$$

So we use (R, x) coordinates in the expressions for:

(i) Volume

$$\begin{aligned}\bar{V} = \pi\int_{\bar{z}_L}^{\bar{z}_R} \bar{r}^2(\bar{z})\mathrm{d}\bar{z} &= \tfrac{4}{3}\pi R_0^3 c^3 \\ &= \frac{\pi}{\sqrt{2}}\int_{-1}^{1} \mathrm{d}x|x|R^3\left\{R^3+\left[R(2x^2-1)-2x(1-x^2)\frac{\mathrm{d}R}{\mathrm{d}x}\right](s-p)\right\} \\ &\quad\times[p+R^2(2x^2-1)+s]^{-\frac{1}{2}}p^{-1}.\end{aligned} \tag{A.6}$$

(ii) Center of mass

$$\begin{aligned}\bar{z}_m = \pi\int_{\bar{z}_L}^{\bar{z}_R} \bar{z}\bar{r}^2(\bar{z})\mathrm{d}\bar{z}/\bar{V} \\ = \frac{\pi}{2}\int_{-1}^{1}\mathrm{d}x\,R^3x\left\{R^3+\left[R(2x^2-1)-2x(1-x^2)\frac{\mathrm{d}R}{\mathrm{d}x}\right](s-p)\right\}p^{-1}/\bar{V}.\end{aligned} \tag{A.7}$$

(iii) The quantity $\bar{Q}$, proportional to the quadrupole moment,

$$\begin{aligned}\bar{Q} &= R_0^{-5}\int_{\bar{z}_L}^{\bar{z}_R}\bar{r}^2(4\bar{z}^2-\bar{r}^2)\mathrm{d}\bar{z} \\ &= \frac{R_0^{-5}}{2\sqrt{2}}\int_{-1}^{1}\mathrm{d}x\,R^3|x|[3p+5R^2(2x^2-1)+5s][p+R^2(2x^2-1)+s]^{-\frac{1}{2}}p^{-1} \\ &\quad\times\left\{R^3+\left[R(2x^2-1)-2x(1-x^2)\frac{\mathrm{d}R}{\mathrm{d}x}\right](s-p)\right\}.\end{aligned} \tag{A.8}$$

(iv) Coulomb potential

$$\begin{aligned}\varphi(r', z') &= \pi\rho_0\int_{z_L}^{z_R} M^{-1}(a, b)\left[f+g\frac{\mathrm{d}r(z)}{\mathrm{d}z}\right]\mathrm{d}z \\ &= \pi\rho_0\int_{-1}^{1}\mathrm{d}x\,M^{-1}(a, b)\left[\left(f\frac{\partial z}{\partial x}+g\frac{\partial r}{\partial x}\right)+\left(f\frac{\partial z}{\partial R}+g\frac{\partial r}{\partial R}\right)\frac{\mathrm{d}R}{\mathrm{d}x}\right],\end{aligned} \tag{A.9}$$

where

$$\begin{aligned} f &= r^2(z)+r'r(z)-\tfrac{1}{2}Q(a, b), \\ g &= (z'-z)r(z), \\ a(r, z) &= \sqrt{(r'+r)^2+(z'-z)^2}, \\ b(r, z) &= \sqrt{(r'-r)^2+(z'-z)^2}, \\ \rho_0 &= \frac{3(Z-1)e}{4\pi R_0^3}, \\ r &= \bar{r}/c, \qquad z = (\bar{z}-\bar{z}_m)/c, \end{aligned} \tag{A.10}$$

and it is implied that $\bar{z}$ and $\bar{r}$ are expressed in terms of x and $R(x)$ by formulae (2); the other quantities in the integral (A.9) and the method of their calculation are described in detail by Strutinsky, Lyashchenko and Popov [8]).

(v) Coulomb energy (in units of the Coulomb energy of the sphere of equal volume)

$$B_c = \frac{3}{8\pi}\rho_0^{-1}R_0^{-5}\int_{z_L}^{z_R}\varphi_s\left(r^2-\tfrac{1}{2}z\frac{dr^2}{dz}\right)dz = \frac{3\sqrt{2}}{8\pi}\rho_0^{-1}R_0^{-5}c^{-3}\int_{-1}^{1}dx\,\varphi_s|x|R^3$$
$$\times\left\{R[R^2+s(2x^2-1)]-2x(1-x^2)s\frac{dR}{dx}\right\}[p+R^2(2x^2-1)+s]^{-\frac{1}{2}}p^{-1}, \quad (A.11)$$

where

$$\varphi_s \equiv \varphi_s[r(R(x),x), z(R(x),x)].$$

(vi) Surface area (in units of the surface area of the sphere of equal volume)

$$B_s = \tfrac{1}{2}R_0^{-2}\int_{z_L}^{z_R} r\left[1+\left(\frac{dr}{dz}\right)^2\right]^{\frac{1}{2}}dz = \frac{1}{2\sqrt{2}}R_0^{-2}c^{-2}\int_{-1}^{1}dx\,R[p-R^2(2x^2-1)-s]^{\frac{1}{2}}$$
$$\cdot\times\left[R^2+(1-x^2)\left(\frac{dR}{dx}\right)^2\right]^{\frac{1}{2}}(1-x^2)^{-\frac{1}{2}}p^{-\frac{1}{2}}. \quad (A.12)$$

In the above expressions

$$\bar{z}_L = -[s+R_0^2(1+\sum_m(-1)^m\alpha_m)^2]^{\frac{1}{2}} = z_L c+\bar{z}_m,$$
$$\bar{z}_R = [s+R_0^2(1+\sum_m\alpha_m)^2]^{\frac{1}{2}} = z_R c+\bar{z}_m.$$

The quantities V, z_m and Q for the normalized curve have the form

$$V = \bar{V}/c^3 = \tfrac{4}{3}\pi R_0^3, \quad (A.13)$$

$$z_m = 0, \quad (A.14)$$

$$Q = c^{-5}(\bar{Q}-4\bar{z}_m^2R_0^{-5}\bar{V}/\pi). \quad (A.15)$$

References

1) V. M. Strutinsky, Yad. Fiz. **3** (1966) 614
2) V. M. Strutinsky, Nucl. Phys. **A95** (1967) 420
3) V. M. Strutinsky, Nucl. Phys. **A122** (1968) 1
4) V. V. Pashkevich, Report JINR (Dubna) R4-4383 (1969)
5) M. Brack, J. Damgaard, H. C. Pauli, A. Stenholm-Jensen, V. M. Strutinsky and C. Y. Wong, Rev. Mod. Phys., to be published
6) S. Cohen and W. J. Swiatecki, Ann. of Phys. **22** (1963) 406
7) V. S. Stavinsky, N. S. Rabotnov and A. A. Seregin, Yad. Fiz. **7** (1968) 1051
8) V. M. Strutinsky, N. Ya. Lyashchenko and N. A. Popov, Nucl. Phys. **46** (1963) 639
9) M. Bolsterli, E. O. Fiset and J. R. Nix, Physics and chemistry of fission (IAEA, Vienna, 1969) p. 183
10) E. Rost, Phys. Lett. **26B** (1968) 184

11) P. E. Nemirovsky, Modern models of the atomic nucleus (Atomizdat, Moscow, 1960)
12) P. E. Nemirovsky and V. A. Chepurnov, Yad. Fiz. **3** (1966) 998
13) V. A. Chepurnov, Yad. Fiz. **6** (1967) 955
14) V. V. Pashkevich and V. M. Strutinsky, Yad. Fiz. **9** (1969) 56
15) J. Damgaard, H. C. Pauli, V. V. Pashkevich and V. M. Strutinsky, Nucl. Phys. **A135** (1969) 432
16) F. A. Gareev, S. P. Ivanova and V. V. Pashkevich, Yad. Fiz. **11** (1970) 1200
17) S. Bjørnholm and V. M. Strutinsky, Nucl. Phys. **A136** (1969) 1
18) S. A. Karamyan, Yu. Ts. Oganesyan and B. I. Pustylnik, Yad. Fiz. **11** (1970) 982
19) H. R. von Gunten, Actinides Review **1** (1969) 275
20) E. P. Steinberg and L. E. Glendenin, in Proc. First Int. Conf. on the peaceful uses of atomic energy **7** (United Nations, New York, 1956) p. 3
21) H. W. Schmitt, J. H. Neiler and F. J. Walter, Phys. Rev. **141** (1966) 1146
22) W. E. Nervik, Phys. Rev. **119** (1960) 1685
23) A. W. Fairhall, R. C. Jensen and F. F. Neusil, Proc. Second U.N. Int. Conf. on the peaceful uses of atomic energy, Geneva, 1958, vol. 15, p. 452
24) T. T. Sugihava *et al.*, Phys. Rev. **121** (1961) 1179
25) P. Möller and S. G. Nilsson, Phys. Lett. **31B** (1970) 283
26) A. V. Ignatyuk, Yad. Fiz. **7** (1968) 1043
27) G. D. Adeev, I. A. Gamalya and P. A. Cherdantsev, Yad. Fiz. **12** (1970) 272